

RobustVisRAG: Causality-Aware Vision-Based Retrieval-Augmented Generation under Visual Degradations

I-Hsiang Chen¹ Yu-Wei Liu¹ Tse-Yu Wu¹ Yu-Chien Chiang¹
Jen-Chieh Yang¹ Wei-Ting Chen²

¹National Taiwan University ²Microsoft

Abstract

Vision-based Retrieval-Augmented Generation (VisRAG) leverages vision-language models (VLMs) to jointly retrieve relevant visual documents and generate grounded answers based on multimodal evidence. However, existing VisRAG models degrade in performance when visual inputs suffer from distortions such as blur, noise, low light, or shadow, where semantic and degradation factors become entangled within pretrained visual encoders, leading to errors in both retrieval and generation stages. To address this limitation, we introduce RobustVisRAG, a causality-guided dual-path framework that improves VisRAG robustness while preserving efficiency and zero-shot generalization. RobustVisRAG uses a non-causal path to capture degradation signals through unidirectional attention and a causal path to learn purified semantics guided by these signals. Together with the proposed Non-Causal Distortion Modeling and Causal Semantic Alignment objectives, the framework enforces a clear separation between semantics and degradations, enabling stable retrieval and generation under challenging visual conditions. To evaluate robustness under realistic conditions, we introduce the Distortion-VisRAG dataset, a large-scale benchmark containing both synthetic and real-world degraded documents across seven domains, with 12 synthetic and 5 real distortion types that comprehensively reflect practical visual degradations. Experimental results show that RobustVisRAG improves retrieval, generation, and end-to-end performance by 7.35%, 6.35%, and 12.40%, respectively, on real-world degradations, while maintaining comparable accuracy on clean inputs. Project page: <https://robustvisrag.github.io/>

1. Introduction

Large language models (LLMs) and vision-language models (VLMs) have shown strong reasoning and generation abilities across diverse tasks [1–3, 23, 26, 65]. However,

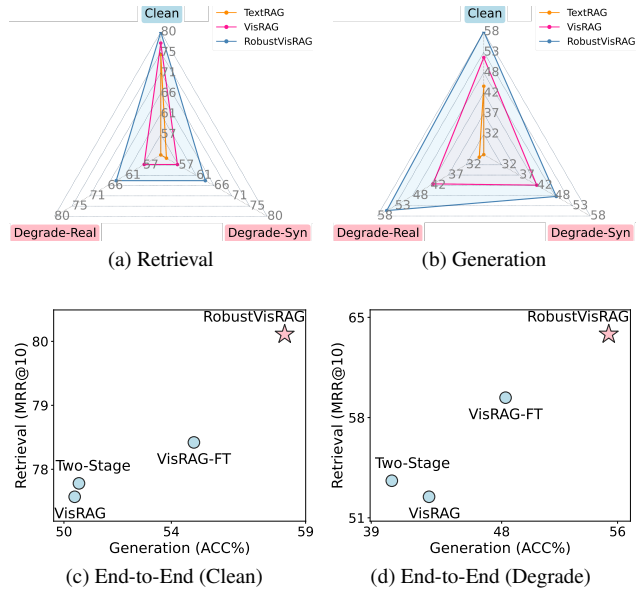


Figure 1. **Illustration of RobustVisRAG’s capabilities.** (a) Retrieval performance under clean, synthetic degradation (Degrade-Syn) and real-degradation (Degrade-Real) scenarios. (b) Generation performance using the retrieved documents from RobustVisRAG as input. (c)(d) End-to-end retrieval-generation performance on clean and degraded data, evaluated under the same baselines including VisRAG, its fine-tuned variants (VisRAG-FT) [45], and a Two-Stage restoration pipeline [42]. Across all settings, both TextRAG and VisRAG show notable performance drops under degraded inputs, whereas RobustVisRAG preserves clean accuracy and significantly improves robustness in degraded conditions.

their parametric nature fixes internal knowledge after training, often leading to hallucinations or outdated predictions [4, 19]. Retrieval-augmented generation (RAG) [14, 22, 61, 62] addresses this limitation by incorporating external knowledge during generation, improving factuality and interpretability. Existing RAG methods can be categorized into Text-based RAG (TextRAG) [14] and Vision-based RAG (VisRAG) [61]. TextRAG operates on textual inputs, retrieving relevant passages for generation. When

document content appears as images, it relies on multi-stage parsing with layout analysis and OCR [29, 41], which accumulates recognition errors [61], discards visual cues, and fails to capture non-textual information such as figures or charts. In contrast, VisRAG leverages VLMs to directly encode visual inputs, avoiding parsing errors and preserving spatial and visual context. This design enables effective multimodal reasoning and alignment during generation.

Although both TextRAG and VisRAG reduce hallucinations and outdated predictions by retrieving external evidence, their performance drops when either the query or the corpus contains degraded document images affected by blur, noise, low light, shadow, or compression artifacts [52], as shown in Fig. 1a and Fig. 1b. In TextRAG, such degradations cause recognition and parsing failures in OCR and layout detection, resulting in incomplete or erroneous retrieval. In VisRAG, visual distortions corrupt the embeddings extracted by VLM encoders, where semantic and distortion factors intertwine, leading to retrieval mismatches and unstable generation. Degradations induce a dual failure mode in the VisRAG pipeline: the model may retrieve incorrect evidence due to corrupted visual representations, and even when the correct evidence is retrieved, degraded inputs can still mislead the generation process. These challenges highlight the need for robustness analysis and mitigation within the VisRAG pipeline under degraded conditions.

To address the above challenges, an intuitive two-stage strategy is to apply existing image restoration techniques [48, 55] to improve the visual quality of degraded images and use the enhanced results as inputs to VisRAG. However, under the degraded VisRAG setting, such restoration-based two-stage pipelines do not consistently translate perceptual improvements into retrieval or generation gains. Alternatively, fine-tuning the VLM itself offers a more direct solution. Parameter-efficient fine-tuning (PEFT) [16] offers a low-cost way to adapt VLMs, but its limited representational capacity hinders effective recovery of degradation-corrupted embeddings. In contrast, full fine-tuning (FFT) enhances adaptability to degraded inputs but requires substantial computational resources and often overfits to distortion patterns while forgetting pretrained knowledge [20]. Moreover, both fine-tuning strategies remain fundamentally limited, as they lack explicit causal guidance to disentangle semantic and distortion factors, which is essential for achieving robust VisRAG under visual degradations. As shown in Fig. 1d, existing two-stage and fine-tuning strategies provide limited performance gains under degraded conditions, highlighting the persistent challenge of distortion robustness in VisRAG.

To address the vulnerability of VisRAG systems under visual degradations, we propose RobustVisRAG, a causality-guided dual-path framework that explicitly separates semantic and degradation information during visual

encoding. RobustVisRAG augments the vision encoder with two complementary pathways: a non-causal path that aggregates degradation cues using a unidirectional attention mechanism, and a causal path that focuses on semantic aggregation and learns purified semantics under the guidance of the degradation signals extracted by the non-causal path. To ensure functional specialization of both pathways, we introduce two learning objectives: Non-Causal Distortion Modeling (NCDM) to enforce structured degradation representation, and Causal Semantic Alignment (CSA) to guide semantic purification and prevent degradation leakage into semantic embeddings. Through joint optimization of these components within a single forward pass, RobustVisRAG effectively disentangles semantic and degradation factors, substantially improving retrieval and generation robustness under degraded visual conditions as shown in Fig. 1.

To evaluate real-world robustness, we construct the Distortion-VisRAG dataset, extending VisRAG [61] with large-scale synthetic and real-world degraded document images. The dataset additionally includes a real-world subset captured under practical conditions such as low light, shadow, and paper damage, narrowing the gap between simulated and natural degradations. The dataset contains 367K question–document pairs across seven document understanding domains (e.g., scientific papers, charts, forms, slides, and handwritten notes), covering 17 degradation types at multiple severity levels. This benchmark enables systematic evaluation of retrieval and generation robustness.

The main contributions of this work are summarized as follows:

- We propose RobustVisRAG, a causality-guided dual-path framework that disentangles semantic and degradation factors during visual encoding to improve VisRAG robustness under degraded conditions without additional inference cost. Extensive experiments show that RobustVisRAG generalizes to real-world degradations in our benchmark, improving retrieval, generation, and end-to-end performance by 7.35%, 6.35%, and 12.40%, respectively, while maintaining comparable performance on clean data.
- We introduce the Distortion-VisRAG dataset, a VisRAG-specific benchmark designed for joint evaluation of retrieval, generation, and end-to-end robustness under synthetic and real-world degradations.

2. Related Work

2.1. Retrieval-Augmented Generation

RAG enhances LLMs by coupling retrieval with generation, grounding answers in external evidence rather than internal parameters [14, 47, 62]. RAG system includes a retriever for locating relevant information and a generator for producing responses based on the query and retrieved context.

Text-based RAG. These methods operate purely on text by applying OCR [18, 29, 41, 66] to document images before retrieval and generation. However, OCR errors and layout loss in complex documents (e.g., tables or charts) cause fragmented information and grounding issues [27, 58], which are further exacerbated under degradations such as blur, noise, or compression [9]. While recent studies [35] suggest that OCR-based pipelines can exhibit competitive robustness under certain document quality conditions, their performance remains sensitive to dataset characteristics and OCR quality.

Vision-based RAG. To address the limitations of text-based RAG, recent studies extend RAG to the visual domain [10, 12, 61]. VisRAG replaces textual modules with vision-language retrievers and generators that encode document images and queries in a shared embedding space, preserving layout and visual cues while reducing OCR errors. However, current models still assume ideal image quality and degrade under real-world conditions, underscoring the need for robustness-oriented VisRAG frameworks.

2.2. VLM Robustness under Degradation

A degradation-robust VLM is essential for reliable VisRAG systems, as both retrieval and generation depend on visual representation quality. Recent studies show that existing VLMs experience performance drops under visual degradations [52]. Although no method is explicitly designed for degradation-aware multimodal learning, prior works have explored potential directions to alleviate this issue, including input enhancement and fine-tuning strategies. One common approach is the two-stage strategy, which enhances input quality before feeding images into the model. Image restoration methods [59, 63] improve perceptual fidelity but may not preserve semantic consistency [5–8], limiting downstream gains. Another approach is fine-tuning: parameter-efficient methods [16] offer lightweight adaptability but limited capacity, while full fine-tuning enhances degraded performance but incurs high computational cost and risks catastrophic forgetting [20], hindering generalization. Moreover, methods such as TeCoA [31] and FARE [45] enhance robustness by adversarially fine-tuning the vision encoders of VLMs, improving their resistance to ℓ_p -bounded perturbations. However, their improvements are confined to small, controllable pixel perturbations and may not generalize to the natural degradations considered here, such as blur, low light, compression, and shadow. Overall, while robustness of VLMs under degradations has been widely studied, robust vision-language understanding within VisRAG pipelines remains underexplored.

2.3. Causality Learning

Causality learning provides a principled framework for understanding the underlying relationships between data at

tributes and model predictions [17, 49, 49]. In vision research, Structural Causal Models have been used to disentangle true semantic causes from spurious correlations, promoting debiasing and domain generalization [30, 54, 57]. Building on this foundation, causal attention [53] and causal prototype learning [28] further incorporate causal reasoning into neural architectures, enhancing interpretability and robustness in visual understanding. Recently, causal reasoning has also been introduced into VLMs to improve compositional reasoning and multimodal alignment [13, 25, 39]. However, these methods mainly operate at the semantic level and assume clean inputs. In real-world scenarios, visual signals are often affected by various forms of visual degradation, which act as latent causal factors that directly influence feature representations. Yet current causal VLM frameworks rarely model this “degradation \rightarrow representation” pathway, leaving semantic features entangled with degradation cues and reducing robustness under real-world conditions.

3. Proposed Method

3.1. Preliminary

Vision-based RAG. Given a textual query q (e.g., a question or instruction) and a visual corpus $\mathcal{V} = \{X_i\}_{i=1}^N$, VisRAG retrieves the top- k most relevant document images and generates a response as follows:

$$\underbrace{R}_{\text{top-}k \text{ retrieved doc images}} = \mathcal{R}(q, \mathcal{E}_r(\mathcal{V})), \quad Y = \mathcal{G}(q, \mathcal{E}_g(R)), \quad (1)$$

where X_i denotes the i -th document image in the corpus, \mathcal{E}_r and \mathcal{E}_g represent the retrieval and generation encoders, and $\mathcal{R}(\cdot)$ and $\mathcal{G}(\cdot)$ denote the retrieval and generation modules, respectively. For notational simplicity, both encoders are hereafter referred to collectively as \mathcal{E}_θ .

In real-world scenarios, document images inevitably suffer from visual degradations such as blur, noise, low light, and shadow, which distort semantics and cause distributional shifts in the embedding space. These degradations reduce retrieval accuracy and propagate errors into the generation stage. Even when correct document images are retrieved, degraded visual inputs can still mislead the generation process, resulting in hallucinated or semantically inconsistent responses. We attribute this issue to *semantic-distortion entanglement*, where semantic and degradation features become intertwined within the visual encoder representations.

Causal Formulation of Degradation in VisRAG. We formalize how semantics and degradations jointly influence VisRAG outputs through a structural causal model (SCM). Let S denote the task-relevant semantic factors, and D denote the degradation (nuisance) factors such as blur or shadow. The observed document image X is generated as

$$X = f(S, D, \varepsilon_X), \quad (2)$$

where $f(\cdot)$ represents the image-formation process and ε_X is an exogenous noise variable. A pretrained vision encoder in VLMs

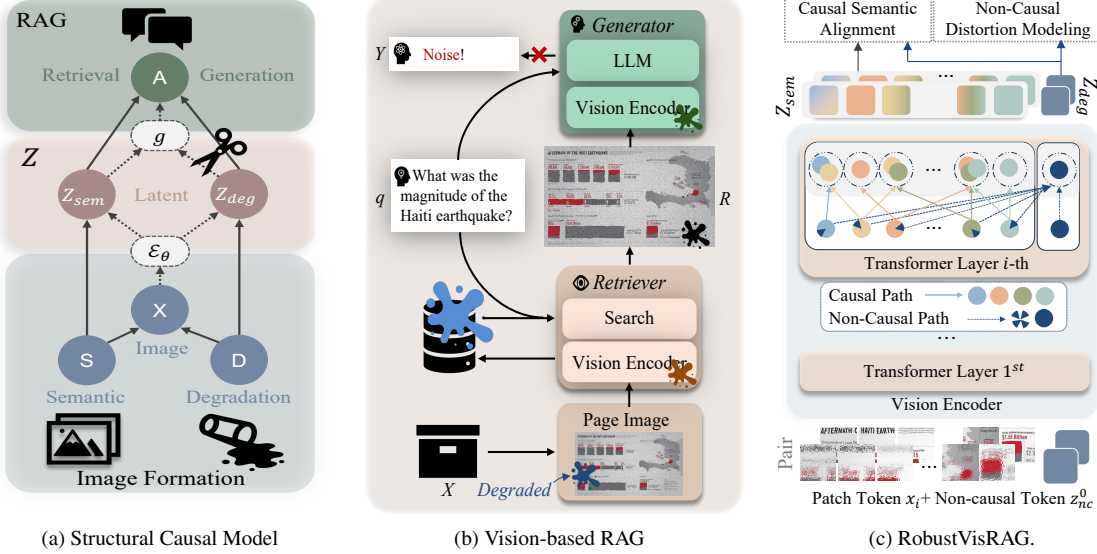


Figure 2. **Overview of RobustVisRAG.** (a) Structural causal model of VisRAG under visual degradations. (b) Architecture of the vanilla vision-based RAG pipeline with degraded input. (c) The proposed RobustVisRAG, which introduces a causality-guided dual-path encoder to disentangle semantic and degradation factors.

\mathcal{E}_θ then maps X into a latent representation:

$$Z = \mathcal{E}_\theta(X), \quad (3)$$

which is further processed by the retrieval and generation modules:

$$(R, Y) = g(q, Z), \quad (4)$$

where $g(\cdot)$ denotes the retrieval and generation mapping in the VisRAG pipeline.

Following the Independent Causal Mechanism principle [46], we assume $S \perp\!\!\!\perp D$ and that all exogenous noise variables are mutually independent. Here, $\perp\!\!\!\perp$ denotes statistical independence. The overall causal structure can be summarized as

$$S \rightarrow X \leftarrow D, \quad X \rightarrow Z, \quad Z \rightarrow (R, Y), \quad (5)$$

where the directed edges represent causal influences between variables. Specifically, S and D jointly determine the observed document image X ; X is then encoded into a latent representation Z by \mathcal{E}_θ ; and Z further drives the retrieval and generation outputs (R, Y) in the VisRAG pipeline. This structure clearly depicts how both semantic and degradation factors propagate through the encoding and reasoning stages. Since Z is a descendant of the collider X , conditioning on Z can open a non-causal path $S \leftrightarrow D$ (\leftrightarrow denotes an induced statistical association), introducing residual dependence $S \not\perp\!\!\!\perp D \mid Z$. Here, $\not\perp\!\!\!\perp$ denotes statistical dependence. This entanglement leads the latent representation Z to mix semantic and degradation information, resulting in corrupted retrieval and unstable generation.

To mitigate this issue, we propose to disentangle the two factors within the latent space. In particular, the representation encoded by \mathcal{E}_θ should preserve task-relevant semantics while isolating degradation cues into a separate subspace. Therefore, our objective is to learn a factorized representation:

$$Z = [Z_{\text{sem}}, Z_{\text{deg}}], \quad (6)$$

where Z_{sem} captures semantic content while Z_{deg} encodes degradation information. Ideally, the representation should satisfy:

$$Z_{\text{sem}} \perp\!\!\!\perp S, \quad Z_{\text{sem}} \perp\!\!\!\perp D. \quad (7)$$

That is, the semantic component should depend only on the causal factors S and remain independent of degradation factors D . Under this condition, the prediction made by the model can be viewed as an approximation of the interventional distribution:

$$P(A \mid do(D = d_0)), \quad A \in \{R, Y\}, \quad (8)$$

where the do-operator $do(\cdot)$ [40] denotes intervention that removes the causal influence of D (e.g., setting D to a reference clean state d_0 , or performing edge surgery to cut $D \rightarrow X$). A as the retrieval and generation outputs (R, Y) . As shown in Fig. 2a, this intervention closes the non-causal path $D \rightarrow X \rightarrow Z \rightarrow A$ while preserving the causal route $S \rightarrow X \rightarrow Z \rightarrow A$. This causal formulation motivates the asymmetric encoder design and the disentanglement objectives introduced in Sec. 3.2. For clarity, we omit the explicit variable X in the following sections, since the encoder \mathcal{E}_θ implicitly maps the observed image X into latent representations $(Z_{\text{sem}}, Z_{\text{deg}})$.

3.2. RobustVisRAG

Overview. Building upon the causal analysis in Sec. 3.1, RobustVisRAG enhances the standard VisRAG pipeline (Fig. 2(b)) with a causality-guided dual-path encoder (Fig. 2(c)). The design explicitly follows the two information sources in the structural causal model: a *non-causal path* that captures degradation factors D , and a *causal path* that encodes task-relevant semantics S . The non-causal path learns to identify and represent degradations through the Non-Causal Distortion Modeling (NCDM) objective, while the causal path leverages these learned degradation cues to

disentangle and purify semantic representations via the Causal Semantic Alignment (CSA) objective. Both paths are jointly optimized in an end-to-end manner, enabling structural intervention on the non-causal route and approximating the interventional behavior $P(A \mid do(D = d_0))$.

Non-Causal Path. To explicitly extract degradation-related information, we introduce a single non-causal token $z_{nc}^{(0)}$ at the input layer. This token is propagated through the network and updated at each layer. Let $\{x_1^{(l)}, \dots, x_T^{(l)}\}$ denote the patch tokens at layer l , and let $z_{nc}^{(l)}$ denote the updated feature of the same non-causal token after layer l . During attention computation, we enforce a directional constraint: (i) the non-causal token is allowed to attend to all patch tokens, and (ii) patch tokens are masked from attending to the non-causal token. Under this design, the non-causal token is updated as

$$z_{nc}^{(l+1)} = z_{nc}^{(l)} + \sum_{j=1}^T \alpha_{nc \leftarrow j}^{(l)} v_j^{(l)}, \quad (9)$$

where $\alpha_{nc \leftarrow j}^{(l)}$ denotes the attention weight from the non-causal token (as query) to the j -th patch token, and $v_j^{(l)}$ is the corresponding value projection.

This unidirectional design lets the non-causal token aggregate degradation cues across spatial regions of the image while preventing these cues from flowing back into the semantic tokens. After L self-attention layers, we obtain the degradation representation:

$$Z_{deg} = z_{nc}^{(L)}. \quad (10)$$

However, structural separation alone does not guarantee that Z_{deg} truly captures degradation factors. Therefore, we further introduce the NCDM objective to explicitly constrain this pathway to focus on degradation modeling while maintaining its non-interference with semantic representations.

Non-Causal Distortion Modeling. The goal of the non-causal path is to encourage a degradation-aware latent subspace. This enables the causal (semantic) branch to utilize such degradation embeddings as guidance for disentanglement within the same forward pass. To achieve this, we introduce a distortion-contrastive objective that enforces degradation-aware discrimination in the latent space. For an anchor image X_a with degradation type d_a , we select a positive sample X_p sharing the same degradation ($d_p = d_a$) and a negative sample X_n with a different degradation ($d_n \neq d_a$), and obtain their degradation embeddings $Z_{deg}^a, Z_{deg}^p, Z_{deg}^n$ from the non-causal path. The objective is formulated as

$$\mathcal{L}_{NCDM} = \max(0, \|Z_{deg}^a - Z_{deg}^p\|_2^2 - \|Z_{deg}^a - Z_{deg}^n\|_2^2 + \delta), \quad (11)$$

where δ is a margin parameter. This contrastive formulation encourages Z_{deg} to cluster samples with the same degradation while separating those from different distortions, thereby encouraging Z_{deg} to encode degradation-consistent patterns that facilitate robustness, without enforcing degradation-type identifiability.

Causal Path. In parallel to the non-causal branch, the causal branch focuses on semantic aggregation through bidirectional attention among patch tokens. The non-causal token is excluded from this attention, so that semantic encoding is not contaminated by degradation-specific features.

Let $x_i^{(l)}$ denote the i -th patch token at layer l , where the subscript c implicitly marks the causal pathway. Given T visual tokens, their update rule is

$$x_i^{(l+1)} = x_i^{(l)} + \sum_{j=1}^T \alpha_{i \leftrightarrow j}^{(l)} v_j^{(l)}, \quad i = 1, \dots, T, \quad (12)$$

where $\alpha_{i \leftrightarrow j}^{(l)}$ is the attention weight between patch tokens only, computed under a mask that removes the non-causal token from both the key and value sets for the causal branch. This formulation is architecture-agnostic: for encoders with a global semantic token [43], that token is included in the patch set and attends to all patches; for pooling-based encoders [64], semantic aggregation arises from contextual interactions among patch tokens.

After L layers, we obtain the semantic representation:

$$Z_{sem} = \text{Agg}(x_1^{(L)}, \dots, x_T^{(L)}), \quad (13)$$

where $\text{Agg}(\cdot)$ denotes the semantic aggregation function used to aggregate patch tokens the underlying encoder architecture. This representation is expected to follow the causal route $S \rightarrow Z_{sem}$ and to remain invariant to degradations. Importantly, Z_{sem} and Z_{deg} are produced simultaneously within the same forward pass: Z_{deg} provides a degradation-related constraint to guide disentanglement during training through the CSA, rather than forming a direct causal dependency on Z_{sem} .

Causal Semantic Alignment. Despite structural separation, early-layer feature sharing may still cause degradation leakage into the causal branch. To explicitly ensure that Z_{sem} captures degradation-invariant semantics, we propose the CSA objective, which leverages Z_{deg} as a causal regulator. For each clean/degraded image pair, we extract Z_{sem}^{clean} from the clean image’s causal path and $(Z_{sem}^{deg}, Z_{deg}^{deg})$ from the degraded image in the same forward pass. We define a joint semantic consistency and independence loss:

$$\mathcal{L}_{SIL} = \frac{1}{T} \sum_{i=1}^T \left[(1 - \langle Z_{sem,i}^{deg}, Z_{sem,i}^{clean} \rangle) + |\langle Z_{sem,i}^{deg}, Z_{deg}^{deg} \rangle| \right], \quad (14)$$

where $\langle \cdot, \cdot \rangle$ denotes cosine similarity and T is the number of semantic tokens. The first term aligns the degraded semantics with the clean semantics, preserving the causal path $S \rightarrow Z_{sem}$, while the second term enforces independence between semantic and degradation embeddings, suppressing the non-causal dependency $D \rightarrow Z_{sem}$. To maintain local structural consistency, we add a fine-grained alignment term:

$$\mathcal{L}_{FSAL} = \frac{1}{T} \sum_{i=1}^T \|Z_{sem,i}^{deg} - Z_{sem,i}^{clean}\|_2^2. \quad (15)$$

The overall CSA objective is given by:

$$\mathcal{L}_{CSA} = \mathcal{L}_{SIL} + \lambda_{FSAL} \mathcal{L}_{FSAL}, \quad (16)$$

where λ_{FSAL} balances global and local alignment. By jointly optimizing \mathcal{L}_{CSA} and \mathcal{L}_{NCDM} , the encoder learns to causally disentangle semantics from degradations within a single forward pass, allowing Z_{sem} to approximate the interventional representation $P(Z_{sem} \mid do(D = d_0))$.

Overall Objective. RobustVisRAG employs two vision encoders for retrieval and generation, both trained under the same causality-guided framework. For retrieval, the encoder is optimized end-to-end with a standard contrastive objective:

$$\mathcal{L}_{\text{Ret}} = -\log \frac{\exp(\langle q, X^+ \rangle / \tau)}{\exp(\langle q, X^+ \rangle / \tau) + \sum_{x^-} \exp(\langle q, X^- \rangle / \tau)}, \quad (17)$$

where X^+ and $\{X^-\}$ denote the positive and negative visual documents to query q , and τ is a temperature. The total retrieval loss combines contrastive learning with causality-guided objectives:

$$\mathcal{L}_{\text{Retrieval}} = \mathcal{L}_{\text{Ret}} + \lambda_1 \mathcal{L}_{\text{CSA}} + \lambda_2 \mathcal{L}_{\text{NCDM}}, \quad (18)$$

where λ_1 and λ_2 balance causal alignment and degradation modeling. For generation, the language model remains frozen while the visual encoder is fine-tuned using only the causality-guided objectives:

$$\mathcal{L}_{\text{Generation}} = \mathcal{L}_{\text{CSA}} + \lambda_3 \mathcal{L}_{\text{NCDM}}, \quad (19)$$

This training allows the adapted encoder to maintain stable semantics under degraded conditions. Through these unified optimization strategies, RobustVisRAG enforces structural intervention to suppress the spurious route $D \rightarrow Z \rightarrow A$ while preserving the causal path $S \rightarrow Z_{\text{sem}} \rightarrow A$.

Inference. At test time, we only require degradation-invariant semantics for retrieval and generation. Since the causal branch already produces Z_{sem} that has been trained to remove degradation information under the guidance of Z_{deg} , we discard the non-causal branch and feed only Z_{sem} to the downstream VisRAG modules. Thus, the inference-time computation and architecture remain compatible with the standard VisRAG pipeline, while enjoying improved robustness to visual degradations.

3.3. Distortion-VisRAG Dataset

We construct the Distortion-VisRAG (DVisRAG) dataset to evaluate the robustness of Vision-based RAG pipelines under degraded visual conditions.¹ It covers seven major document VQA domains, including scientific papers, charts, slides, infographics, forms, handwritten notes, and reports, and contains a total of 367,608 question–document (Q–D) pairs. The dataset consists of two complementary parts: the Synthetic Degradation Dataset and the Real-World Degradation Dataset, corresponding to synthetic and real degradation scenarios, respectively. The synthetic subset includes 362,110 training samples and 3,607 testing samples, while the real subset contains 1,891 testing samples.

Synthetic Degradation Dataset. This subset is built upon VisRAG [61], encompassing all its original data sources, including ArXivQA [24], ChartQA [32], PlotQA [34], InfoVQA [33], MP-DocVQA [51], SlideVQA [50] and Synthetic [61]. Following the degradation synthesis pipeline in UniRestore [5], we generate twelve common types of degradation (e.g., blur, noise, brightness variation, color saturation change, and resolution reduction), each at five severity levels. For each image in the dataset, we randomly sample one degradation type and one severity level to synthesize

¹More details on dataset statistics, collection procedures, and degradation generation methods are provided in the supplementary material.

the degraded version. The training and testing splits are identical to those of VisRAG, and all question–answer pairs remain unchanged. Only the document images are degraded to ensure full comparability and consistent evaluation settings.

Real Degradation Dataset. This subset is designed to evaluate model generalization under real-world conditions. We randomly sample a portion of Q–D pairs from the ArXivQA and MP-DocVQA test sets of VisRAG, and additionally include document samples from RVL-CDIP [15], yielding 1,891 non-overlapping test pairs. All documents are printed and photographed using a Sony RX100 VII camera under controlled capture settings, such as varying shutter speed, exposure compensation, and partial illumination occlusion, to create five real degradation types: blur, low light, low resolution, shadow, and paper damage. This dataset is used exclusively for testing and does not participate in training.

4. Experiments

We conduct experiments to validate the effectiveness of RobustVisRAG. Due to space limitations, detailed implementation settings and more experimental results are provided in the supplementary material.

4.1. Implementation Details.

RobustVisRAG adopts the same backbone as VisRAG [61], using MiniCPM-V 2.0 [61] as the retriever and MiniCPM-V 2.6 [38] as the generator. Both components are initialized from pre-trained checkpoints and fine-tuned under the mixed-dataset setting, which combines the training splits of the VisRAG and DVisRAG datasets. Evaluation is conducted on three test sets: the VisRAG test split, the synthetic degradation subset, and the real degradation subset from DVisRAG. Following VisRAG [61], we report MRR@10 (Mean Reciprocal Rank at 10) for retrieval ranking quality and Accuracy for generation performance, where the latter adopts a relaxed 5% numerical tolerance to account for rounding and OCR errors.

4.2. Baselines

Following the evaluation protocol of VisRAG [61], we evaluate RobustVisRAG across three stages: retrieval, generation, and end-to-end. Baseline methods are categorized into two types: (i) text-based pipelines that apply OCR [11] to extract textual content from document images and then perform retrieval or generation based on recognized text, and (ii) vision-based pipelines that directly process raw images without textual conversion. Text-based methods are marked with “(T)”, while unmarked ones are vision-based.

For retrieval, we consider multiple representative backbones, including BM25 (T) [44], BGE-large (T) [56], NV-Embed-v2 (T) [21], SigLIP [64], and ColPali [12]. We also include MiniCPM-V2.0 [61], which serves as the retrieval backbone in VisRAG and is denoted as VisRAG-Ret. For generation, we adopt several representative models, including MiniCPM (T) [37, 60], and GPT-4o [36]. We further include MiniCPM-V2.6 [38, 60], which serves as the generation backbone in VisRAG and is denoted as VisRAG-Gen.

To systematically analyze robustness and adaptation behavior, we introduce three configurations as follows. All models are fine-tuned following the official settings described in their respective

Table 1. Overall retrieval performance (MRR@10) on the VisRAG and the DVisRAG datasets. “Synthetic” and “Real” denote results on the synthetic-degradation and real-degradation subsets of the DVisRAG dataset.

Models	# Para.	DVisRAG Dataset	
		VisRAG Dataset	Synthetic Real
BM25 (T)	n.a	53.34	32.80 38.60
BGE-large (T)	335M	58.98	37.05 35.23
NV-Embed-v2 (T)	7.85B	72.41	47.68 49.44
MiniCPM-FV (T)	2.72B	74.94	48.54 52.09
MiniCPM-FM (T)	2.72B	73.17	49.96 51.72
SigLIP	883M	43.47	33.10 15.07
SigLIP-FV	883M	71.52	57.51 28.50
SigLIP-FM	883M	68.84	59.77 31.89
ColPali-FV	2.97B	74.57	61.22 41.70
VisRAG-Ret	3.43B	77.57	65.96 56.47
VisRAG-Ret-FM	3.43B	78.39	68.69 58.25
VisRAG-Ret-FM (FARE)	3.43B	<u>78.42</u>	<u>69.11</u> <u>59.39</u>
RobustVisRAG	3.43B	80.11	73.21 63.82

Table 2. Overall generation performance (Accuracy) on the VisRAG and the DVisRAG datasets.

Models	Metric	DVisRAG Dataset	
		VisRAG Dataset	Synthetic Real
GPT-4o (T)	top-1	44.05	26.26 27.61
	top-2	47.44	29.51 28.73
	top-3	47.03	30.63 29.44
	Oracle	53.06	37.90 41.54
MiniCPM (T)	top-1	28.44	18.58 18.21
	top-2	28.43	18.06 20.07
	top-3	27.79	18.18 18.80
	Oracle	31.92	24.23 25.22
GPT-4o	top-1	52.44	43.31 41.49
	top-2	53.69	45.29 44.08
	top-3	54.98	45.74 44.81
	Oracle	<u>63.50</u>	54.52 58.61
VisRAG-Gen	top-1	51.51	42.16 44.70
	top-2	53.82	43.35 47.15
	top-3	54.11	44.53 47.14
	Oracle	63.36	51.52 62.68
VisRAG-Gen-FM (PEFT)	top-1	53.92	43.64 47.22
	top-2	55.44	44.51 48.82
	top-3	55.22	45.18 49.35
	Oracle	64.88	53.16 <u>63.52</u>
VisRAG-Gen-FM (FFT)	top-1	<u>55.50</u>	44.44 47.29
	top-2	<u>56.32</u>	45.92 49.59
	top-3	55.68	46.17 49.03
	Oracle	<u>65.91</u>	53.20 62.54
VisRAG-Gen-FM (FARE)	top-1	55.49	<u>45.68</u> <u>50.95</u>
	top-2	<u>56.87</u>	<u>47.75</u> <u>53.14</u>
	top-3	<u>57.02</u>	48.18 <u>53.46</u>
	Oracle	<u>66.13</u>	<u>54.69</u> <u>64.46</u>
RobustVisRAG	top-1	58.22	48.02 55.39
	top-2	60.98	53.18 57.91
	top-3	61.99	54.01 59.44
	Oracle	67.33	57.87 69.03

papers, ensuring consistent optimization protocols.

(i) **Vanilla Models.** Pre-trained models are directly evaluated without any fine-tuning to assess their zero-shot capability.

(ii) **Fine-tuned on VisRAG Dataset.** Following the official VisRAG training protocol [61], models are fine-tuned on the VisRAG dataset using in-domain question–document supervision, denoted as “-FV”.

(iii) **Fine-tuned on Mixed Dataset.** Models are fine-tuned jointly on the VisRAG dataset and our DVisRAG dataset, denoted as “-FM”.

Table 3. End-to-end retrieval–generation performance on VisRAG and DVisRAG datasets.

Methods	Retrieval (MRR@10)			Generation (Top-1)		
	VisRAG Dataset	Synthetic	Real	VisRAG Dataset	Synthetic	Real
VisRAG	77.57	65.96	56.47	50.40	41.96	42.99
VisRAG-FT	78.42	69.11	59.39	54.84	44.96	48.27
Two-Stage	77.78	66.49	53.59	50.56	42.25	40.42
RobustVisRAG	80.11	73.21	63.82	58.22	48.02	55.39

4.3. Overall Results and Analysis

Retrieval Performance. As shown in Tab. 1, RobustVisRAG achieves the best retrieval performance across all datasets. Compared with the original VisRAG-Ret, RobustVisRAG improves retrieval accuracy by 2.54% on clean data and by 7.25% and 7.35% under synthetic and real degradations. We also compare against VisRAG-FARE, which applies adversarial robustness training to VisRAG-Ret. Even under this stronger baseline, RobustVisRAG achieves further gains of +1.69%, +4.10%, and +4.43% on the clean, synthetic, and real subsets, respectively. Three observations emerge under our setting. First, vision-based retrieval is inherently more stable under degradations, while OCR-dependent pipelines suffer from noise, blur, and illumination artifacts. Second, mixed-dataset fine-tuning (-FM) consistently improves degraded-domain performance, though its effect on clean accuracy varies across architectures. Third, adversarial robustness training yields limited improvement under the complex degradations scenarios in DVisRAG dataset. In contrast, RobustVisRAG explicitly disentangles semantic and degradation factors, leading to robustness that generalizes consistently across all visual conditions.

Generation Performance. We evaluate various generation models using the retrieval results obtained from RobustVisRAG. Note that in the original VisRAG [61], only the retriever was fine-tuned, while the generation module (VisRAG-Gen) remained frozen. To further investigate how generator adaptation affects robustness, we fine-tune VisRAG-Gen under three strategies: Full Finetuning (denoted as “-FFT”), PEFT [16] (denoted as “-PEFT”), and adversarial robustness training following FARE [45] (denoted as “-FARE”).

We report results using the top-1, top-2, and top-3 retrieved documents, as well as under the Oracle setting, where the model is given access only to the ground-truth positive document. As shown in Tab. 2, RobustVisRAG consistently outperforms all existing methods across different settings, achieving stable improvements on both synthetic and real-world degraded datasets. Specifically, RobustVisRAG improves over VisRAG-Gen by 6.35% under the Oracle setting and surpasses GPT-4o by 10.42%. Among the fine-tuning strategies, FARE achieves better robustness than FFT and PEFT due to its additional feature-space alignment constraint, which helps the model resist local perturbations. However, its improvement remains limited since such alignment does not explicitly disentangle semantic and degradation representations. In contrast, RobustVisRAG leverages degradation features extracted from the non-causal path as guidance to explicitly separate these factors during training, achieving stronger semantic stability and degradation invariance across both clean and corrupted inputs.

End-to-End Performance. We further evaluate the complete retrieval–generation pipeline to assess the end-to-end robustness

Table 4. Ablation on different configurations of RobustVisRAG on DVisRAG dataset.

Configurations	Retrieval (MRR@10)		Generation (Top-1)	
	Synthetic	Real	Synthetic	Real
Baseline	65.96	56.47	41.96	42.99
RobustVisRAG w/o U	69.12	60.28	45.34	49.54
RobustVisRAG w/o $\mathcal{L}_{\text{NCDM}}$	69.20	61.94	47.21	51.79
RobustVisRAG w/o \mathcal{L}_{CSA}	67.48	58.24	44.96	45.72
RobustVisRAG w/o $\mathcal{L}_{\text{NCDM}}$ & \mathcal{L}_{CSA}	66.34	56.94	42.94	43.80
RobustVisRAG	73.21	63.82	48.02	55.39

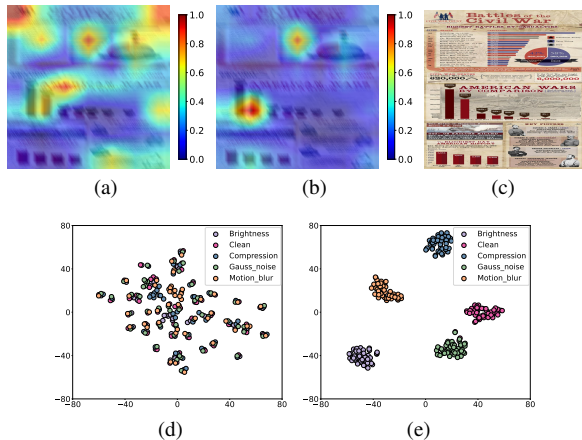


Figure 3. Comparison of token representations under degradations: Attention visualizations of (a) VisRAG and (b) RobustVisRAG. (c) Clean version corresponding to (a) and (b). t-SNE visualization of Z_{deg} from (d) RobustVisRAG w/o $\mathcal{L}_{\text{NCDM}}$ & \mathcal{L}_{CSA} and (e) RobustVisRAG.

of RobustVisRAG compared with VisRAG-based configurations. Since VisRAG [61] and RobustVisRAG share identical retrieval and generation backbones, their differences lie solely in training and adaptation strategies. We include the following variants for comparison: (i) the vanilla VisRAG (denoted as *VisRAG*); (ii) the best-performing VisRAG finetuning configuration combining VisRAG-Ret-FM (FARE) and VisRAG-Gen-FM (FARE) (denoted as *VisRAG-FT*); and (iii) a two-stage enhancement strategy, where degraded images are first restored using image restoration method [42] before being fed into the vanilla VisRAG pipeline (denoted as *Two-Stage*).

As shown in Tab. 3, RobustVisRAG outperforms all baselines under degraded conditions while maintaining comparable accuracy to the vanilla VisRAG in clean settings. On real-world degraded datasets, RobustVisRAG achieves an average improvement of 7.35% in the retrieval stage and further raises the end-to-end accuracy by 12.4%, indicating that the benefits of semantic-degradation disentanglement effectively propagate through the entire pipeline. In contrast, the two-stage enhancement strategy, though conceptually intuitive, offers limited gains since the restoration step may distort clean images and does not ensure downstream robustness under degraded conditions.

4.4. Ablation Study

To analyze the contribution of each component, we train all variants on the mixed dataset and evaluate them on both the VisRAG and DVisRAG test sets.

Effectiveness of Proposed Modules. We design six configurations to analyze the contribution of each component: (i) Baseline: the original VisRAG framework; (ii) RobustVisRAG w/o U: replacing the unidirectional Non-Causal Path with a bidirectional connection. This setting is equivalent to adding a Non-Causal Token into the VisRAG architecture but training it jointly with the two objectives $\mathcal{L}_{\text{NCDM}}$ and \mathcal{L}_{CSA} , without enforcing directional separation; (iii) RobustVisRAG w/o $\mathcal{L}_{\text{NCDM}}$: removing the non-causal degradation modeling objective; (iv) RobustVisRAG w/o \mathcal{L}_{CSA} : removing the causal semantic alignment objective; (v) RobustVisRAG w/o $\mathcal{L}_{\text{NCDM}}$ & \mathcal{L}_{CSA} : removing both loss terms simultaneously; (vi) RobustVisRAG: the full model with all proposed modules. As shown in Tab. 4, all components contribute to improved robustness and generalization. The unidirectional attention constraint is essential for preventing semantic-degradation entanglement and preserving a clear causal separation between the two pathways, as evidenced by the comparison between (ii) and (vi). The comparison between (v) and (vi) further shows that adding a Non-Causal Path alone is insufficient; without the two proposed objectives, it fails to learn meaningful degradation features and yields only limited gains. Overall, the results demonstrate that each module in RobustVisRAG is necessary.

Investigation of Learned token representations. To analyze how degradations affect semantic encoding, we conduct two complementary visualization studies. First, we sample a degraded image from DVisRAG and use the text query “Bar Chart”. We compute the similarity between the text embedding and the mean patch-token features, then project the similarity map back onto the image. As shown in Fig. 3(a)(b), RobustVisRAG focuses more consistently on semantically relevant regions, whereas vanilla VisRAG is easily disrupted by degradations and tends to highlight irrelevant areas. This indicates that RobustVisRAG learns semantic representations that are significantly more degradation-invariant.

Next, we sample 50 image-question-answer triplets and apply five types of synthetic degradations to each image. We then compare the degradation representations using the Z_{deg} features from RobustVisRAG and from the variant RobustVisRAG w/o $\mathcal{L}_{\text{NCDM}}$ & \mathcal{L}_{CSA} . As shown in Fig. 3(c)(d), the variant without these objectives exhibits poor separability among degradation types, whereas RobustVisRAG produces clear and compact clusters. This demonstrates that the combined effect of NCDM and CSA encourages degradation-consistent structure in the latent space.

5. Conclusion

We presented RobustVisRAG, a VisRAG-oriented causality-guided dual-path framework that mitigates retrieval-generation error propagation under degradations. Through structural design and targeted objectives, RobustVisRAG improves retrieval, generation, and end-to-end performance under degradations while preserving clean-data accuracy. These gains come with no additional inference cost. We also introduce the Distortion-VisRAG dataset, a comprehensive benchmark for evaluating multimodal RAG models under degraded visual conditions.

References

- [1] Josh Achiam, Steven Adler, Sandhini Agarwal, et al. Gpt-4 technical report. *arXiv preprint arXiv:2303.08774*, 2023. 1
- [2] Jean-Baptiste Alayrac, Jeff Donahue, Pauline Luc, Antoine Miech, Iain Barr, Yana Hasson, Karel Lenc, Arthur Mensch, Katherine Millican, Malcolm Reynolds, et al. Flamingo: a visual language model for few-shot learning. *NeurIPS*, 2022.
- [3] Jinze Bai, Shuai Bai, Shusheng Yang, Shijie Wang, Sinan Tan, Peng Wang, Junyang Lin, Chang Zhou, and Jingren Zhou. Qwen-vl: A versatile vision-language model for understanding, localization, text reading, and beyond. *arXiv preprint arXiv:2308.12966*, 2023. 1
- [4] Yejin Bang, Samuel Cahyawijaya, Nayeon Lee, et al. A multitask, multilingual, multimodal evaluation of chatgpt on reasoning, hallucination, and interactivity. In *AAACL-IJCNLP*, 2023. 1
- [5] I Chen, Wei-Ting Chen, Yu-Wei Liu, Yuan-Chun Chiang, Sy-Yen Kuo, Ming-Hsuan Yang, et al. Unirestore: Unified perceptual and task-oriented image restoration model using diffusion prior. In *CVPR*, 2025. 3, 6
- [6] I-Hsiang Chen, Hua-En Chang, Wei-Ting Chen, Jenq-Neng Hwang, Sy-Yen Kuo, et al. Exploring probabilistic modeling beyond domain generalization for semantic segmentation. In *ICCV*, 2025.
- [7] Wei-Ting Chen, I-Hsiang Chen, Chih-Yuan Yeh, Hao-Hsiang Yang, Hua-En Chang, Jian-Jiun Ding, and Sy-Yen Kuo. Rvsl: Robust vehicle similarity learning in real hazy scenes based on semi-supervised learning. In *ECCV*, 2022.
- [8] Wei-Ting Chen, I-Hsiang Chen, Chih-Yuan Yeh, Hao-Hsiang Yang, Jian-Jiun Ding, and Sy-Yen Kuo. Sjd-vehicle: Semi-supervised joint defogging learning for foggy vehicle re-identification. In *AAAI*, 2022. 3
- [9] Jane Courtney. Sediqa: Sound emitting document image quality assessment in a reading aid for the visually impaired. *Journal of Imaging*, 2021. 3
- [10] Yihao Ding, Siwen Luo, Hyunsuk Chung, and Soyeon Caren Han. Pdfvqa: A new dataset for real-world vqa on pdf documents. In *Proceedings of ECML PKDD 2023*, 2023. 3
- [11] Yuning Du, Chenxia Li, Ruoyu Guo, et al. Pp-ocr: A practical ultra lightweight ocr system. *arXiv preprint arXiv:2009.09941*, 2020. 6
- [12] Manuel Faysse, Hugues Sibille, Tony Wu, Gautier Viaud, Céline Hudelot, and Pierre Colombo. Colpali: Efficient document retrieval with vision language models. *arXiv preprint arXiv:2407.01449*, 2024. 3, 6
- [13] Mengyu Gao and Qiulei Dong. Causality-guided prompt learning for vision-language models via visual granulation. *arXiv preprint arXiv:2509.03803*, 2025. 3
- [14] Kelvin Guu, Kenton Lee, Zora Tung, Panupong Pasupat, and Ming-Wei Chang. Retrieval augmented language model pre-training. In *ICML*, 2020. 1, 2
- [15] Adam W Harley, Alex Ufkes, and Konstantinos G Derpanis. Evaluation of deep convolutional nets for document image classification and retrieval. In *ICDAR*, 2015. 6
- [16] Edward J Hu, Yelong Shen, Phillip Wallis, Zeyuan Allen-Zhu, Yuanzhi Li, Shean Wang, Lu Wang, and Weizhu Chen. Lora: Low-rank adaptation of large language models. *ICLR*, 2022. 2, 3, 7
- [17] Guido W Imbens and Donald B Rubin. *Causal inference in statistics, social, and biomedical sciences*. Cambridge University Press, 2015. 3
- [18] Guillaume Jaume, Hazim Kemal Ekenel, and Jean-Philippe Thiran. Funsd: A dataset for form understanding in noisy scanned documents. In *ICDAR Workshops*, 2019. 3
- [19] Ziwei Ji, Nayeon Lee, Rita Frieske, et al. Survey of hallucination in natural language generation. *ACM Comput. Surv.*, 2023. 1
- [20] Gangwei Jiang, Zhaoyi Li, Defu Lian, and Ying Wei. Refine large language model fine-tuning via instruction vector. *arXiv preprint arXiv:2406.12227*, 2024. 2, 3
- [21] Chankyu Lee, Rajarshi Roy, Mengyao Xu, Jonathan Raiman, Mohammad Shoeybi, Bryan Catanzaro, and Wei Ping. Nv-embed: Improved techniques for training llms as generalist embedding models. *arXiv preprint arXiv:2405.17428*, 2024. 6
- [22] Patrick S. H. Lewis, Ethan Perez, Aleksandra Piktus, Fabio Petroni, Vladimir Karpukhin, Naman Goyal, Heinrich Küttler, Mike Lewis, Wen-tau Yih, Tim Rocktäschel, Sebastian Riedel, and Douwe Kiela. Retrieval-augmented generation for knowledge-intensive nlp tasks. In *NeurIPS*, 2020. 1
- [23] Junnan Li, Dongxu Li, Caiming Xiong, and Steven Hoi. Blip: Bootstrapping language-image pre-training for unified vision-language understanding and generation. In *ICML*, 2022. 1
- [24] Lei Li, Yuqi Wang, Runxin Xu, Peiyi Wang, Xiachong Feng, Lingpeng Kong, and Qi Liu. Multimodal arxiv: A dataset for improving scientific comprehension of large vision-language models. *ACL*, 2024. 6
- [25] Zhiyuan Li, Heng Wang, Dongnan Liu, Chaoyi Zhang, Ao Ma, JiETING Long, and Weidong Cai. Multimodal causal reasoning benchmark: Challenging vision large language models to discern causal links across modalities. In *Findings of ACL*, 2025. 3
- [26] Haotian Liu, Chunyuan Li, Qingyang Wu, and Yong Jae Lee. Visual instruction tuning. In *NeurIPS*, 2023. 1
- [27] Ye Liu, Kazuma Hashimoto, Yingbo Zhou, Semih Yavuz, Caiming Xiong, and Philip S. Yu. Dense hierarchical retrieval for open-domain question answering. In *EMNLP*, 2021. 3
- [28] Yajing Liu, Shijun Zhou, Xiyao Liu, Chunhui Hao, Baojie Fan, and Jiandong Tian. Unbiased faster r-cnn for single-source domain generalized object detection. In *CVPR*, 2024. 3
- [29] Chuwei Luo, Yufan Shen, Zhaoqing Zhu, Qi Zheng, Zhi Yu, and Cong Yao. Layoutllm: Layout instruction tuning with large language models for document understanding. In *CVPR*, 2024. 2, 3
- [30] Fangrui Lv, Jian Liang, Shuang Li, Bin Zang, Chi Harold Liu, Ziteng Wang, and Di Liu. Causality inspired representation learning for domain generalization. In *CVPR*, 2022. 3
- [31] Chengzhi Mao, Scott Geng, Junfeng Yang, Xin Wang, and Carl Vondrick. Understanding zero-shot adversarial robustness for large-scale models. *arXiv preprint arXiv:2212.07016*, 2022. 3
- [32] Ahmed Masry, Do Xuan Long, Jia Qing Tan, Shafiq Joty, and Enamul Hoque. Chartqa: A benchmark for question an-

- swering about charts with visual and logical reasoning. *ACL*, 2022. 6
- [33] Minesh Mathew, Viraj Bagal, Rubèn Tito, Dimosthenis Karatzas, Ernest Valveny, and CV Jawahar. Infographicvqa. In *WACV*, 2022. 6
- [34] Nitesh Methani, Pritha Ganguly, Mitesh M Khapra, and Pratyush Kumar. Plotqa: Reasoning over scientific plots. In *WACV*, 2020. 6
- [35] Alexander Most, Joseph Winjum, Manish Bhattarai, Shawn Jones, Nishath Rajiv Ranasinghe, Ayan Biswas, and Dan O’Malley. Lost in ocr translation? vision-based approaches to robust document retrieval. In *ACM DocEng*, 2025. 3
- [36] OpenAI. Hello, gpt-4o, 2024. 6
- [37] OpenBMB. openbmb/minicpm-v-2, 2024. 6
- [38] OpenBMB. openbmb/minicpm-v-2_6, 2024. 6
- [39] Fiorenzo Parascandolo, Nicholas Moratelli, Enver Sangineto, Lorenzo Baraldi, and Rita Cucchiara. Causal graphical models for vision-language compositional understanding. In *ICLR*, 2025. 3
- [40] Judea Pearl, Madelyn Glymour, and Nicholas P Jewell. *Causal inference in statistics: A primer*. John Wiley & Sons, 2016. 4
- [41] Birgit Pfitzmann, Christoph Auer, Michele Dolfi, Ahmed Samy Nassar, and Peter W. J. Staar. Doclaynet: A large human-annotated dataset for document-layout analysis. In *Proceedings of the 28th ACM SIGKDD Conference on Knowledge Discovery and Data Mining*, pages 3743–3751, 2022. 2, 3
- [42] Vaishnav Potlapalli, Syed Waqas Zamir, Salman H Khan, and Fahad Shahbaz Khan. PromptIR: Prompting for all-in-one image restoration. In *Advances in Neural Information Processing Systems (NeurIPS)*, 2023. 1, 8
- [43] Alec Radford, Jong Wook Kim, Chris Hallacy, et al. Learning transferable visual models from natural language supervision. In *ICML*, 2021. 5
- [44] Stephen E Robertson, Steve Walker, Susan Jones, Micheline M Hancock-Beaulieu, Mike Gatford, et al. Okapi at trec-3. In *TREC-3*, 1995. 6
- [45] Christian Schlarman, Naman Deep Singh, Francesco Croce, and Matthias Hein. Robust clip: Unsupervised adversarial fine-tuning of vision embeddings for robust large vision-language models. *ICML*, 2024. 1, 3, 7
- [46] Bernhard Schölkopf, Francesco Locatello, Stefan Bauer, et al. Toward causal representation learning. *IEEE Signal Process. Mag.*, 2021. 4
- [47] Weijia Shi, Sewon Min, Michihiro Yasunaga, Minjoon Seo, Richard James, Mike Lewis, Luke Zettlemoyer, and Wentaoh Yih. Replug: Retrieval-augmented black-box language models. In *HLT*, 2024. 2
- [48] Taeyoung Son, Juwon Kang, Namyup Kim, Sunghyun Cho, and Suha Kwak. Urie: Universal image enhancement for visual recognition in the wild. In *ECCV*, 2020. 2
- [49] Peter Spirtes, Clark N Glymour, and Richard Scheines. *Causation, prediction, and search*. MIT Press, 2000. 3
- [50] Ryota Tanaka, Kyosuke Nishida, Kosuke Nishida, Taku Hasegawa, Itsumi Saito, and Kuniko Saito. Slidevqa: A dataset for document visual question answering on multiple images. In *AAAI*, 2023. 6
- [51] Rubèn Tito, Dimosthenis Karatzas, and Ernest Valveny. Hierarchical multimodal transformers for multipage docvqa. *Pattern Recognition*, 2023. 6
- [52] Muhammad Usama, Syeda Aishah Asim, Syed Bilal Ali, Syed Talal Wasim, and Umair Bin Mansoor. Analysing the robustness of vision-language-models to common corruptions. *arXiv preprint arXiv:2504.13690*, 2025. 2, 3
- [53] Tan Wang, Chang Zhou, Qianru Sun, and Hanwang Zhang. Causal attention for unbiased visual recognition. In *ICCV*, 2021. 3
- [54] Yunqi Wang, Furui Liu, Zhitang Chen, Yik-Chung Wu, Jianye Hao, Guangyong Chen, and Pheng-Ann Heng. Contrastive-ace: Domain generalization through alignment of causal mechanisms. *TIP*, 2022. 3
- [55] Cong Wei, Yang Chen, Haonan Chen, et al. Uniir: Training and benchmarking universal multimodal information retrievers. *arXiv preprint arXiv:2311.17136*, 2023. 2
- [56] Shitao Xiao, Zheng Liu, Peitian Zhang, Niklas Muennighoff, Defu Lian, and Jian-Yun Nie. C-pack: Packaged resources to advance general chinese embedding. *arXiv preprint arXiv:2309.07597*, 2023. 6
- [57] Mingjun Xu, Lingyun Qin, Weijie Chen, Shiliang Pu, and Lei Zhang. Multi-view adversarial discriminator: Mine the non-causal factors for object detection in unseen domains. In *CVPR*, 2023. 3
- [58] Peng Xu, Wei Ping, Xianchao Wu, et al. Chatqa 2: Bridging the gap to proprietary llms in long context and rag capabilities. *arXiv preprint arXiv:2407.14482*, 2024. 3
- [59] Zizheng Yang, Jie Huang, Jiahao Chang, Man Zhou, Hu Yu, Jinghao Zhang, and Feng Zhao. Visual recognition-driven image restoration for multiple degradation with intrinsic semantics recovery. In *CVPR*, 2023. 3
- [60] Yuan Yao, Tianyu Yu, Ao Zhang, Chongyi Wang, Junbo Cui, Hongji Zhu, et al. Minicpm-v: A gpt-4v level mllm on your phone. *arXiv preprint arXiv:2408.01800*, 2024. 6
- [61] Shi Yu, Chaoyue Tang, Bokai Xu, Junbo Cui, Junhao Ran, et al. Visrag: Vision-based retrieval-augmented generation on multi-modality documents. *ICLR*, 2025. 1, 2, 3, 6, 7, 8
- [62] Zichun Yu, Chenyan Xiong, Shi Yu, and Zhiyuan Liu. Augmentation-adapted retriever improves generalization of language models as generic plug-in. In *ACL*, 2023. 1, 2
- [63] Syed Waqas Zamir, Aditya Arora, Salman Khan, Munawar Hayat, Fahad Shahbaz Khan, Ming-Hsuan Yang, and Ling Shao. Multi-stage progressive image restoration. In *CVPR*, 2021. 3
- [64] Xiaohua Zhai, Basil Mustafa, Alexander Kolesnikov, and Lucas Beyer. Sigmoid loss for language image pre-training. In *ICCV*, 2023. 5, 6
- [65] Wayne Xin Zhao, Kun Zhou, Junyi Li, et al. A survey of large language models. *arXiv preprint arXiv:2303.18223*, 2023. 1
- [66] Xu Zhong, Jianbin Tang, and Antonio Jimeno Yepes. Publaynet: Largest dataset ever for document layout analysis. In *ICDAR*, 2019. 3